Bayesian Optimization of Interconnect Flow-Field Design for Mitigating In-plane Temperature Gradients in Solid Oxide Electrolysis Cells

Hoseob Lee [a], Hyeyeong Jun [a], Yonggyun Bae [b*], Mingi Choi [a*]

a Department of Future Energy Convergence, Seoul National University of Science and Technology, Seoul 01811, Republic of Korea
b Department of Zero-Carbon Fuel and Power Generation, Eco-Friendly Energy Conversion Research Division, Korea Institute of Machinery & Materials (KIMM), Daejeon 34103, Republic of Korea
**Corresponding author*
Email address: mgchoi@seoultech.ac.kr (Mingi Choi)
Email address: ygbae@kimm.re.kr (Yonggyun Bae)

Abstract:

This study proposes a hybrid optimization framework combining high-fidelity computational fluid dynamics (CFD), Gaussian process (GP) surrogate modeling, and ε-Pareto Active Learning (ε-PAL) for efficient multi-objective optimization of solid oxide electrolysis cell (SOEC) operation. Key operating variables, including flow rates and gas compositions, are considered due to their strong impact on electrochemical performance and thermal behavior. The closed-loop framework iteratively integrates CFD results with GP predictions to estimate objective values and uncertainties, enabling ε-PAL to selectively sample uncertain and Pareto-relevant regions. This approach significantly reduces computational cost while efficiently exploring the design space. The results show simultaneous improvement in voltage efficiency and reduction in temperature gradients, demonstrating that the proposed framework effectively identifies optimal trade-offs under limited simulation budgets.

Keywords:

Active-learning; Computational Fluid Dynamics; Multi-objective function; Solid Oxide Electrolysis Cell.

1. Introduction

Solid oxide electrolysis cells (SOECs) have been considered as promising energy conversion device for hydrogen production which can offer high efficiency at high temperatures (>700–800 °C) due to its enhanced electrode reaction kinetics and thermodynamic advantages. When assisted by external heat sources for steam generation, SOECs can achieve hydrogen production efficiencies exceeding 95% on a higher heating value (HHV) basis, while reducing hydrogen production costs through lower electrical energy consumption[1].

Recent studies have emphasized that, although SOECs exhibit high efficiency potential at both the stack and system levels, challenges related to large-area scaling, operating strategies for maintaining high efficiency, stability improvement, and thermal management remain key hurdles to commercialization. However, since SOECs involve strong coupling among electrochemical reactions, fluid flow, species transport, and heat transfer, these multiphysics interactions directly affect not only performance and efficiency but also thermal and mechanical reliability [2]. Accordingly, multiphysics analysis has become increasingly important for understanding SOEC behavior.

Among the durability indicators of SOECs, temperature non-uniformity and thermal gradients have been consistently recognized as critical factors. Recent multiphysics studies have shown that the temperature distribution and thermal stress inside SOECs can vary significantly depending on operating conditions, flow-field configuration, current density, and feed composition. Large thermal gradients and thermal stresses can significantly contribute to structural damage and performance degradation. In particular, three-dimensional computational fluid dynamics (CFD)-structural coupled models and stack-level simulations have demonstrated that non-uniformities in temperature and current density distributions can lead to localized increases in thermal stress [3, 4].

Therefore, the exploration of SOEC operating conditions should be formulated as a multi-objective optimization problem, balancing high efficiency and low thermal gradients. For example, operating conditions that maximize voltage efficiency do not necessarily guarantee low in-plane thermal gradients. At the same

time, thermally stable conditions with uniform temperature distribution do not always correspond to the highest efficiency point. Under such competing objectives, identifying the Pareto front is more appropriate than searching for a single optimum. However, the design and operating space of SOECs is both continuous and high-dimensional, and the evaluation of each candidate condition generally requires either costly experiments or high-fidelity CFD simulations. Thus, exploration of all possible combinations is computationally inefficient. This limitation has also been widely recognized in broader materials and process discovery problems, where there is a strong need for computational strategies that minimize expensive evaluations while efficiently identifying promising solutions [3].

In this regard, Gaussian process (GP) based active learning, Bayesian optimization, have attracted significant attention as suitable methodologies for expensive engineering problems. In particular, GP models provide not only predictions of objective values at unevaluated design points but also associated predictive uncertainty, making them highly advantageous for sequentially selecting the most informative candidates under limited evaluation budgets. Accordingly, for multi-objective problems, Pareto Active Learning (PAL)-type methods have been proposed. Zuluaga et al. introduced ε-PAL as a framework for actively identifying an epsilon-accurate Pareto set [4]. More recently, Adaptive ε-PAL has extended this framework to continuous spaces by employing tree-based adaptive discretization. In this approach, the GP posterior is used to classify the design space into discarded, undecided, and predicted Pareto regions, thereby enabling the identification of an ε-accurate Pareto set with a minimal number of evaluations. This approach is particularly well suited to problems in which the entire Pareto front must be efficiently approximated over a continuous design space.

Although multiphysics studies combining experiments and simulations have been actively conducted in the SOEC field, studies that construct a GP-based active learning framework using experimentally validated three-dimensional CFD data and systematically explore the Pareto front with respect to the conflicting objectives of maximizing voltage efficiency and minimizing in-plane thermal gradients remain limited. Existing SOEC optimization studies have often focused on a single performance metric, comparison of a limited number of operating conditions, or mechanistic interpretation under predefined simulation settings. In contrast, sample-efficient identification of Pareto-optimal operating regions over a continuous design space has not yet been sufficiently explored. To address this gap, the present study employs an experimentally validated ANSYS Fluent-based SOEC CFD model as a high-fidelity evaluator and constructs an active learning loop in which the resulting data are sequentially incorporated into a GP surrogate model. On this basis, voltage efficiency maximization and in-plane thermal gradient minimization are formulated as two objective functions, and Adaptive epsilon-PAL is applied to efficiently explore the Pareto front in a continuous operating-condition space. The proposed approach aims to reduce the computational burden associated with high-fidelity SOEC simulations while quantitatively characterizing the trade-off between electrochemical performance and thermal stability.

The objective of this study is to combine an experimentally validated high-fidelity SOEC CFD model with GP-based active learning in order to efficiently identify the Pareto front between voltage efficiency and in-plane thermal gradients under a limited simulation budget. To this end, a GP surrogate model is constructed using multiphysics simulation results obtained from ANSYS Fluent, and Adaptive epsilon-PAL is employed to progressively refine promising operating regions in the continuous design space. Through this framework, the present work proposes a data-efficient optimization methodology for systematically analyzing the thermo-electrochemical trade-off in SOEC operation.

2. Methodology

2.1 Numerical modeling

The numerical analysis was performed using the finite volume method in the commercial CFD software ANSYS Fluent 2025 R2 with the Fuel Cell and Electrolysis add-on module. The computational domain was discretized into 654,200 cells, and the minimum element edge length was 3×10^{-6} m. To ensure spatial accuracy, local mesh refinement was introduced in the through-thickness direction of the cell, especially near the electrode-electrolyte interfaces and in regions with large gradients in reaction rates and thermophysical properties. For the numerical solution, laminar flow was assumed, the pressure-velocity coupling was treated using the SIMPLE algorithm, and second-order upwind schemes were applied to all governing equations. The simulations were conducted on a workstation equipped with an Intel Core i7-14700K CPU and 32 GB of RAM, with parallel computation performed using two CPU cores. Solution convergence was assessed from the residuals, and residual levels of 10^{-4}, 10^{-11}, and 10^{-9} were obtained for continuity, energy, and species, respectively. Accordingly, the computational time required for a single operating condition at 0.5 A/cm^2 was approximately 3 h 30 min.

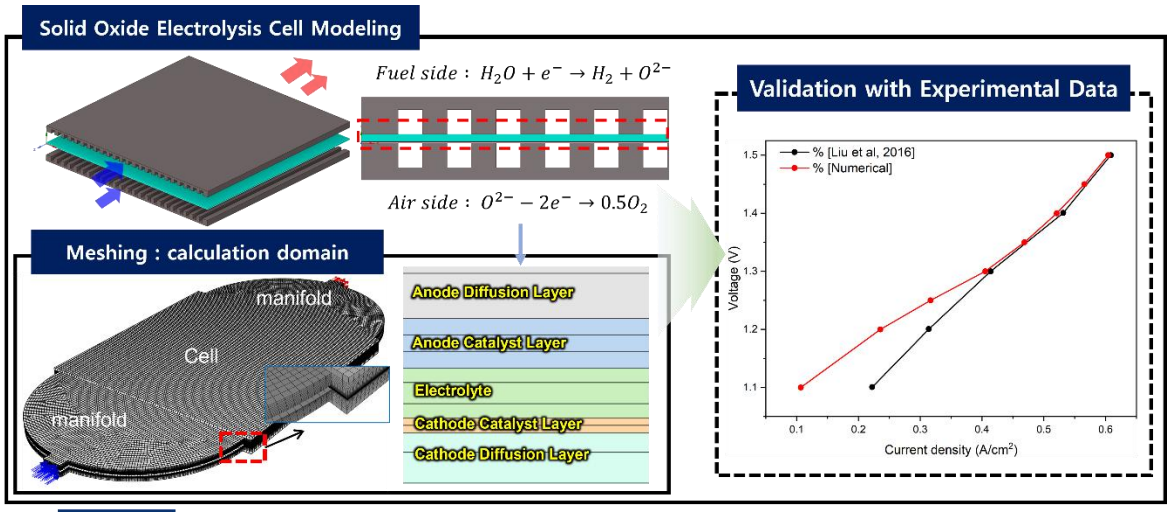

Figure 1. SOEC model for CFD calculation and validation [5].

Table 1. Computational modeling domain dimensions of SOEC.

Geometry and operational parameters	value	units
Length and width	50	mm
Anode Diffusion Layer thickness	400	μm
Anode Catalyst Layer thickness	10	μm
Electrolyte thickness	10	μm
Cathode Catalyst Layer thickness	3	μm
Cathode Current Collector Layer thickness	30	μm
Steam and Air channel height	1	mm
Steam and Air channel width	1	mm

Table 2. Materials properties of the cell and interconnect.

Materials properties	Anode NiO/YSZ	Electrolyte YSZ	Cathode LSM	Interconnect Metal
Specific heat [J/kg·K]	450	450	450	450
Thermal conductivity [W/m·K]	10	2	11	72
Electron conductivity [1/Ωm]	333,330	-	7973	1.5×10^7
Density [kg/m^3]	6500	5480	5620	8900
Tortuosity	5	-	5	-
porosity	0.5	-	0.5	-
Anode contact resistance [Ωm^2]	-	-	-	3e-06
Cathode contact resistance [Ωm^2]	-	-	-	3e-06

2.2 Mathematical formulation

Table 3. Governing equations for CFD calculations of SOEC.

Mass conservation	$(\nabla \cdot (\rho \boldsymbol{u}) = S_m)$
Momentum conservation	$(\nabla \cdot (\rho \boldsymbol{u}\boldsymbol{u}) = -\nabla p + \nabla \cdot (\mu \nabla \boldsymbol{u}) + \boldsymbol{S_{mom}})$
Species conservation	$(\nabla \cdot (\rho \boldsymbol{u} Y_i) = -\nabla \cdot \boldsymbol{J_i} + S_i)$
Species diffusion flux	$\left(J_i = \text{-}\rho D_{i,eff}\, \nabla Y_i\right)$
Effective diffusion coefficient (porous zone)	$\left(D_{i,\text{eff}} = \frac{\varepsilon}{\tau} D_i\right)$
Knudsen-diffusion	$\left(\frac{1}{D^*_{i,\text{eff}}} = \frac{1}{D_{i,\text{eff}}} + \frac{1}{D_{K,i}}\right)$
Energy conservation	$(\nabla \cdot (\rho \boldsymbol{u} h) = \nabla \cdot (k_{\text{eff}} \nabla T) + S_E)$
Charge conservation (electronic phase)	$(\nabla \cdot (\sigma_s \nabla \phi_s) = -S_{ct})$
Charge conservation (ionic phase)	$(\nabla \cdot (\sigma_{ion} \nabla \phi_{ion}) = S_{ct})$
Nernst potential	$\left(E_{\text{Nernst}} = E^0 + \frac{RT}{nF} \ln\left(\frac{a_{\text{products}}}{a_{\text{reactants}}}\right)\right)$
Butler–Volmer	$\left(i = i_0 \left[\exp\left(\frac{\alpha_a F \eta_{act}}{RT}\right) - \exp\left(\frac{\alpha_c F \eta_{act}}{RT}\right)\right]\right)$
Exchange current density (Concentration dependence)	$\left(i_0 = i_{0,\text{ref}} \left(\frac{X_{H_2}}{X_{H_2,\text{ref}}}\right)^{\gamma_{H_2}} \left(\frac{X_{H_2O}}{X_{H_2O,\text{ref}}}\right)^{\gamma_{H_2O}} \left(\frac{X_{O_2}}{X_{O_2,\text{ref}}}\right)^{\gamma_{O_2}}\right)$
Exchange current density (Temperature dependence)	$\left(i_0(T) = A \exp\left(-\frac{B}{T}\right)\right)$
Activation overpotential	$(\eta_{act} = \phi_s - \phi_{ion} - E_{\text{Nernst}})$
Ohmic overpotential	$\left(\eta_{ohm} = iR_{ohm} = i \frac{L_{ely}}{\sigma_{ion}}\right)$
Electrical conductivity and Resistivity	$\left(\rho_{ely} = f(T),\ \sigma_{ion} = \frac{1}{\rho_{ely}}\right)$
Ohmic heat source	$\left(q_{\text{ohm}} = \frac{\lvert \boldsymbol{i} \rvert^2}{\sigma}\right)$
Electrochemical heat source	$(q_{\text{echem}} = i\eta_{act})$

2.3 Boundary conditions

Table 4. Boundary conditions for Operating parameter.

	Position	value		Unit
Mass flow rate	Inlet channel (co-flow)	Mass flow rate inlet (steam/air)	2.18×10^{-6}/ 1.18×10^{-6}	kg/s
		H_2O mole fraction	0.1-0.9	-
		H_2 mole fraction	0.1-0.9	-
Operating temperature	Steam, air channel inlet		1073	K
Wall	All faces	Heat flux	0	
	Terminal Anode	Specific value	0	V
	Terminal Cathode	Specific value	1.1-1.5	V

2.4 Model validation

The developed SOEC model was validated compared to the experimental data reported in the literature to ensure its predictive capability. The reference study investigated a planar SOEC under operating conditions comparable to those considered in the present work, including temperature ranges in 1073-1273 (K), gas compositions in 10-90 (%), and current densities at 1.1-1.5 (V).[6] For validation, the simulated polarization curves were compared with the experimental results. The model predictions showed good agreement with the experimental data, corresponding to the operating current-density range considered in this study. The error between the experimental and simulated results was 0.41-1.05 %, remaining within 3 % throughout the range. For same boundary conditions, in this study, flow boundary conditions corresponding to 25 % of the cell size ($10 \times 10\ cm^2$) reported in the relevant paper were used for the ($5 \times 5\ cm^2$) cell analysis (Fuel utilization rate is 43 %). These results confirm that the present model can reliably capture the electrochemical and thermal behavior of the SOEC system and thus can be used for subsequent multi-objective optimization and Pareto analysis.

2.5 Active learning method

To efficiently utilize computationally expensive 3D CFD simulations, an active learning-based sequential sampling strategy was adopted in this study. The design space consists of multidimensional continuous operating variables that govern the thermo-fluidic and electrochemical behavior of the SOEC, including the fuel- and air-side flow rates, steam composition at the fuel electrode inlet, and oxygen composition at the air electrode inlet. Each combination of these variables defines a single operating condition within the continuous design space. Since the response at each operating condition must be evaluated through high-fidelity 3D CFD simulations, exhaustive exploration of the entire design space is computationally prohibitive.

Therefore, rather than uniformly sampling the full operating space, the present study employs an active learning strategy that sequentially prioritizes operating conditions predicted to be either highly uncertain or particularly influential in shaping the Pareto front, thereby reducing the number of expensive evaluations required to identify the Pareto set.

2.5.1 Surrogate model

Active learning was performed by sequentially selecting the next CFD evaluation point based on the predictive mean $\mu_{i,t}(x)$ and uncertainty $\sigma_{i,t}^2(x)$ of a Gaussian process (GP) surrogate model. Let $data\ D_t$ denote the set of CFD data accumulated up to iteration t. For an operating condition x, the GP posterior of the i-th objective function $f_i(x)$ is expressed as

$$f_i(x)\big|D_t \sim \mathcal{GP}(\mu_{i,t}(x)\,, \sigma_{i,t}^2(x) \qquad \text{Eq.(1)}$$

The covariance function of the Gaussian process was defined as a combination of a constant kernel, a Matérn kernel, and a white-noise kernel. The overall kernel function is given by

$$k(x, x') = \sigma_f^2 k_{Matérn}(x, x') + \sigma_n^2 \delta_{xx'} \qquad \text{Eq.(2)}$$

Where σ_f^2 denotes the signal variance, σ_n^2 represents the noise variance, and $\delta_{xx'}$ is the Kronecker delta. The $Matérn$ kernel was specified with $\nu = 1.5$, for which the kernel function can be written as.

$$k_{Matérn}(x, x') = \left(1 + \sqrt{3}r\right)exp\left(-\sqrt{3}r\right),\ r = \sqrt{\sum_{j=1}\left(\frac{x_j - x_j'}{\ell_j}\right)^2} \qquad \text{Eq.(3)}$$

Here, ℓ_j denotes the length scale associated with the j input variable. Independent length scales were assigned to each input dimension in order to capture differences in variable sensitivity. This allows the GP model to learn the heterogeneous influence of operating variables on the objective functions.

The $Matérn$ kernel was adopted because it can flexibly represent the nonlinear and locally varying behavior commonly observed in engineering systems. In particular, $\nu = 1.5$ implies that the response function is continuous but not excessively smooth, which is suitable for describing the multiphysics CFD response characteristics of SOECs. In addition, the white-noise term was included to improve numerical stability and to account for residual error or modeling noise contained in CFD-based data. Prior to GP training, all input variables were normalized to the range [0,1], which improves the stability of kernel hyperparameter optimization and facilitates interpretation of the learned length scales across input variables.

2.6 Epsilon-Pareto active learning (ε-PAL)

The multi-objective function vector at an operating condition x is defined as

$$f(x) = \left(f_1(x), f_2(x)\right) \qquad \text{Eq.(4)}$$

Based on $\mu_{i,t}(x), \sigma_{i,t}^2(x)$, the confidence interval bounds for each point can be defined as follows.

$$L(x) = \mu(x) - \sqrt{\beta}\sigma(x),\ U(x) = \mu(x) + \sqrt{\beta}\sigma(x) \qquad \text{Eq.(5)}$$

ε-PAL is an ε-dominance relationship as follows.

$$y + \varepsilon \geq y' \qquad \text{Eq.(6)}$$

Using the ε-dominance relation, ε-PAL removes points satisfying $U(x) \leq L_\varepsilon(x')$ from the pareto candidate set and selects the point with the largest uncertainty as the next evaluation point. This procedure continues until the remaining candidate set forms an ε-accurate Pareto set with high probability. Since the SOEC operating space is continuous, the present study follows the rationale of Adaptive ε-PAL, which uses tree-based adaptive discretization to refine only uncertain or promising regions, thereby reducing the number of expensive CFD evaluations required for Pareto set identification.

3. Results and discussion

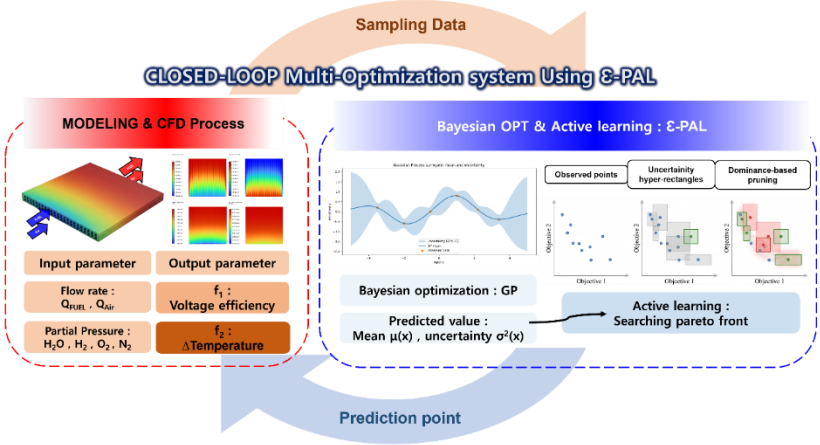

Figure 2. Multi-objective Active Learning with CFD Process in Closed-Loop system.

Figure 2 shows the ε-PAL–CFD hybrid framework for the multi-objective optimization. The parameter space is defined as a multidimensional continuous operating space consisting of the fuel flow rate (Q_{FUEL}, sccm), the air flow rate (Q_{Air}, sccm), the steam composition at the fuel electrode (P_{H_2O}), and the oxygen composition at the air electrode (P_{O_2}). Since voltage efficiency and in-plane thermal gradient significantly vary with these operating variables, exhibiting an inherent multi-objective trade-off, multi-objective optimization process has to be considered to achieve both high efficiency and stability.

The closed-loop scheme illustrated in Figure 2 integrates high-fidelity CFD analysis, Gaussian process (GP) surrogate modeling, and ε-PAL-driven active learning in an iterative manner. An initial set of CFD results is first employed to construct the GP model, which estimates both performance metrics and their associated uncertainties across unexplored design regions. Leveraging these estimations, ε-PAL determines subsequent operating points for CFD evaluation by focusing on areas with high uncertainty or potential Pareto optimality. Each newly obtained CFD outcome is incorporated into the dataset, followed by continuous refinement of the GP model. Through this iterative cycle, the framework efficiently uncovers the operating trade-offs of the SOEC system while minimizing computational cost.

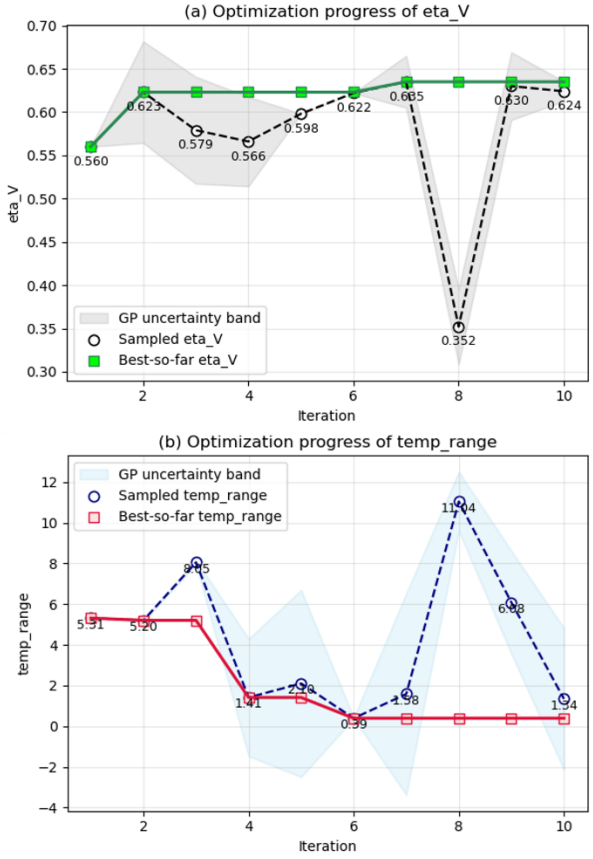

Figure 3. Iterative optimization process in terms of (a) voltage efficiency and (b) temperature difference.

$$\eta_{el,SOEC} = 1 - \frac{V_{overpotential}}{V_{OCV}} \qquad \text{Eq.(7)}$$

$$\Delta T = T_{Max} - T_{Min} \qquad \text{Eq.(8)}$$

First, we define the voltage efficiency and temperature difference as Eq. (7) and (8), respectively. Figure 3 shows the iterative optimization progress in terms of voltage efficiency and temperature difference. Each objective is predicted using a GP-based surrogate model, which provides both the predicted objective values and the associated predictive uncertainties for unevaluated operating conditions. This enables the algorithm to preferentially sample regions with high predictive uncertainty or a high likelihood of belonging to the Pareto front, thereby reducing unnecessary CFD evaluations. In Figure 3 (a, b), the dashed line represents the

sampled values at each iteration, the colored solid line indicates the cumulative best-observed value, and the gray shaded region denotes the GP predictive mean along with the corresponding uncertainty band of ±1.96σ. As the iterations proceed, the best-observed value of voltage efficiency gradually increases, while the minimum temperature-difference decreases, indicating that the framework progressively identifies operating conditions with improved electrochemical performance and thermal stability. Overall, voltage efficiency improves by 14%, whereas the temperature difference is reduced by 80% within 10 iterations compared to the initial condition. Therefore, we could confirm that the ε-PAL-based active learning–CFD hybrid framework provides an effective and computationally efficient approach for multi-objective optimization of SOEC operation, enabling systematic exploration of performance–stability trade-offs in a high-dimensional design space.

4. Conclusions

In this work, an $\boldsymbol{\varepsilon}$-PAL–CFD hybrid framework was developed to address the multi-objective optimization of SOEC operating conditions, considering both voltage efficiency and thermal stability. By coupling high-fidelity CFD simulations with GP-based surrogate modeling and uncertainty-driven active learning, the proposed approach enables efficient exploration of a complex, high-dimensional operating space. The iterative optimization results confirm that the framework successfully improves electrochemical performance while simultaneously mitigating thermal gradients, demonstrating its capability to capture the inherent trade-offs between competing objectives. Notably, significant performance enhancement was achieved within a limited number of iterations, indicating a substantial reduction in computational burden compared to conventional exhaustive simulation approaches. Overall, the proposed methodology provides a systematic and computationally efficient strategy for SOEC operation optimization. Furthermore, the framework is readily extendable to other electrochemical energy systems and multi-physics optimization problems, offering a versatile platform for accelerating design and operational decision-making in advanced energy technologies.

Acknowledgments

This research was supported by the National research Foundation of Korea (NRF) grant funded by the Korea Government (MSIT) (No. RS-2026-25486899) and Korea Institute of Energy Technology Evaluation and Planning (KETEP) grant funded by the Korea government (MCEE)(RS-2025-16066396).

References

[1] Tu, Y., et al., *The study of multiphysics field coupling and thermal stress in three types of Solid Oxide Electrolysis Cells (SOEC).* International Journal of Electrochemical Science, 2024. **19**(10): p. 100789.

[2] Iyer, S., et al., *Review of experimental and modelling investigations for solid oxide electrolysis technology.* International Journal of Hydrogen Energy, 2024. **72**: p. 537–558.

[3] Liu, C., Z. Dang, and G. Xi, *Numerical study on thermal stress of solid oxide electrolyzer cell with various flow configurations.* Applied Energy, 2024. **353**: p. 122041.

[4] Zuluaga, M., et al. *Active learning for multi-objective optimization*. in *International conference on machine learning*. 2013. PMLR.

[5] Liu, T.-L., et al., *Evaluation of polarization and hydrogen production efficiency of solid oxide electrolysis stack with La0. 6Sr0. 4Co0. 2Fe0. 8O3− δ-Ce0. 9Gd0. 1O1. 95 oxygen electrode.* International Journal of Hydrogen Energy, 2016. **41**(36): p. 15970–15978.

[6] Hasbi, S., et al., *Performance optimisation of solid oxide electrolyser cell (SOEC) using response surface method (RSM) for thermal gradient reduction.* International Journal of Sustainable Energy, 2025. **44**(1): p. 2482837.